CP-21

Proceedings of the **1996 ASME IMECE**
Second International Symposium on Multiphase Flows and Heat Transfer in Materials Processing
Atlanta, Georgia --- November 17-22, 1996

HTD-Vol. 336/FED-Vol. 240
Transport Phenomena in Materials Processing and Manufacturing
ASME 1996, pp. 275-282

SIMULATION OF MICRO-PORE FORMATION IN SPRAY DEPOSITION PROCESSES

J.-P. Delplanque, E.J. Lavernia, and R.H. Rangel

Department of Mechanical and Aerospace Engineering
and
Department of Chemical Engineering and Materials Science
University of California, Irvine
Irvine, California

ABSTRACT

The present work investigates porosity formation in spray deposition processes. The emphasis is on one possible mechanism of micro-pore formation during droplet spreading and solidification: liquid-jet overflow. To this end, the Navier-Stokes equations are solved numerically using finite differences and the free surface is tracked using the Volume Of Fluid method. A previously developed multi-directional solidification algorithm is adapted and implemented in the Navier-Stokes solver to perform numerical simulations of liquid-metal droplet impact, spreading, and solidification. The results obtained allow a detailed description of the liquid-jet overflow mechanism and of the resulting solidified disk morphology. The influence of the Weber and Reynolds numbers, the solidification constant, and the contact angle is investigated.

NOMENCLATURE

c	contact angle
D	droplet diameter
F	volume of fluid function
$\overline{\boldsymbol{F_g}}$	body forces
$\overline{\boldsymbol{g}}$	gravity acceleration
h_{sf}	latent heat of solidification
k	thermal conductivity
p	pressure
Pe	$= \mathcal{V}D/\alpha$, Peclet number
Re	$= \mathcal{V}D/\nu$, Reynolds number
s	curvilinear coordinate
$\mathcal{S}$	local position of solidified layer
Ste	$= k\Delta T/(\alpha\rho h_{sf})$ Stefan number
T	temperature
t	time
$\overline{\boldsymbol{V}}$	velocity vector
$\mathcal{V}$	droplet impact velocity
We	$= \rho\mathcal{V}^2 D/\sigma$, Weber number
r	radial coordinate
y	axial coordinate

Greek symbols

α	thermal diffusivity
γ	solid fraction
θ	volume fraction open to flow
σ	surface tension coefficient
ρ	density
λ	solidification constant
ν	kinematic viscosity

Subscripts

ℓ	liquid
s	solid or substrate

Diacritics

—	vector

INTRODUCTION

Spray deposited materials (using spray forming, plasma spraying, and other droplet processes) usually exhibit a larger amount of non-interconnected porosity than materials produced using more conventional processes, ingot casting for instance. Depending on the type of end-use that the material is intended for, it may be desired to minimize porosity (higher strength and resistance to cyclic deformation) or to enhance it (better thermal insulation, noise damping, and crush resistance). Therefore, controlling the

porosity of spray deposited materials is an important goal as it would significantly widen their possible range of applications.

The understanding of porosity formation during spray deposition has improved over the past few years. Extensive microstructural characterizations have provided a classification of the various types of pores found in spray-deposited materials (Lavernia and Wu, 1995), and formation mechanisms have been proposed; gas entrapment (Benz *et al.*, 1994), solidification shrinkage (Cai *et al.*, 1994), and interstitial porosity (Lavernia, 1989). Much remains to be done however; some mechanisms have not yet been identified and the existing knowledge remains quite phenomenological. Further insight can be obtained through an improved mechanistic understanding of droplet impact, spreading, and solidification. Because the thrust of relevant research efforts has hitherto been experimental (Lavernia, 1989; Zhang *et al.*, 1993; Sampath and Herman, 1993; Orme, 1993; Passow *et al.*, 1993; Inada and Yang, 1994; Sobolev and Guilemany, 1994), it is hoped that supplementary and edifying information can be provided by numerical simulations. Indeed, this motivation is at the source of recent endeavors to simulate these phenomena (Trapaga *et al.*, 1992; Liu *et al.*, 1993; Fukai *et al.*, 1993; Liu *et al.*, 1994).

The objective of the present work is to provide a quantitative insight into porosity formation during droplet spreading and solidification. We focus more particularly on one possible mechanism of micro-pore formation; liquid-jet overflow. This phenomenon has been identified through numerical simulations (Liu *et al.*, 1994; Delplanque *et al.*, 1995) and observed experimentally (Inada and Yang, 1994). Liquid-jet overflow occurs when the high-velocity liquid metal flowing on top of the solidifying disk overflows and forms a liquid layer which extends radially without touching the substrate. This liquid layer re-attaches at a farther radial location where solidification also starts. Our goal here is to provide a detailed understanding of this mechanism and to identify the relative influences of the Weber and Reynolds numbers, the solidification constant, and the contact angle.

MODEL DESCRIPTION

In order to simulate accurately the impact, spreading, and solidification of a liquid-metal droplet on a colder substrate (cf. Fig. 1) it is necessary to solve the full Navier-Stokes equations and track both the deforming liquid free-surface and the growing solid/liquid interface. The model presented herein combines a 2D axisymmetric Navier-Stokes solver for fluid flow with free surfaces (RIPPLE) developed at the Los Alamos National Laboratory (Kothe and Mjolsness, 1992) and a multi-directional solidification algorithm developed by the authors (Delplanque *et al.*, 1995). The fluid flow equations:

$$\nabla \cdot \left(\theta \overline{\boldsymbol{V}}\right) = 0 \tag{1}$$

$$\theta \frac{\partial \overline{\boldsymbol{V}}}{\partial t} + \nabla \cdot \left(\theta \, \overline{\boldsymbol{V}} \, \overline{\boldsymbol{V}}\right) = -\frac{\theta}{\rho} \nabla p + \frac{\theta}{\rho} \nabla \cdot \tau + \theta \overline{\boldsymbol{g}} + \theta \overline{\boldsymbol{F}}_b \tag{2}$$

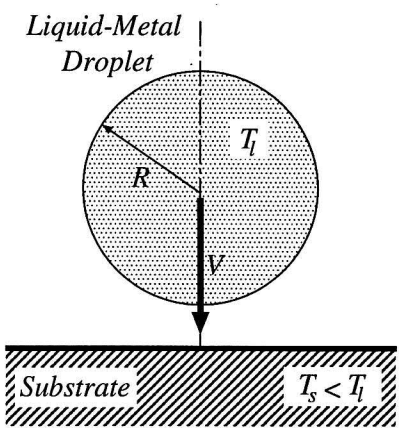

FIGURE 1: GEOMETRY OF THE PROBLEM. DROPLET IMPACT, SPREADING, AND SOLIDIFICATION.

are solved using a two-step projection method, including an incomplete Cholesky conjugate gradient solution of the pressure Poisson equation. θ is a function which characterizes the presence of the growing solid which acts as an obstacle internal to the solution domain (θ= 1 in the fluid or void and 0 in obstacles). The distribution of the liquid is given by a Volume of Fluid transport equation:

$$\frac{\partial}{\partial t}\left(\theta F\right) + \nabla \cdot \left(\theta F \overline{\boldsymbol{V}}\right) = 0 \tag{3}$$

where F is the Volume of Fluid function (F= 1 in the fluid and 0 in the void). Surface tension effects are modeled using the continuum surface force approach. More details concerning RIPPLE may be found in Kothe and Mjolsness (1992) .

The solidification process is described using a locally 1D multi-directional algorithm (Delplanque *et al.*, 1995). The solid/liquid interface is tracked in a Lagrangian manner using uniformly distributed markers. The displacement of each marker is evaluated assuming that the solidification process can be approximated locally by the solution to a modified Stefan solidification problem:

$$\frac{\partial \mathcal{S}}{\partial t} = \frac{2\lambda^2 \alpha_s}{\mathcal{L}} \tag{4}$$

where $\mathcal{L}$ is the shortest distance to the substrate and the solidification constant, λ, is obtained from a heat balance at the interface:

$$\lambda = \frac{1}{\sqrt{\pi}} \left\{ \frac{\mathrm{Ste}_s}{\mathrm{erf}\left[\lambda\right] \exp(\lambda^2)} - \frac{\mathrm{Ste}_\ell \sqrt{\alpha_\ell / \alpha_s}}{\mathrm{erf}\left[\lambda \sqrt{\alpha_s / \alpha_\ell}\right] \exp\left[\lambda^2 \alpha_s / \alpha_\ell\right]} \right\} \tag{5}$$

where Ste_s and Ste_ℓ are the solid and liquid Stefan numbers. More advanced heat transfer models including substrate remelt-

ing are currently being developed by our group (Rangel and Bian, 1996). For a time increment of Δt, each marker is therefore displaced along the local normal to the solid/liquid interface by:

$$\Delta \mathcal{S} = \frac{\partial \mathcal{S}}{\partial t} \Delta t \tag{6}$$

The algorithm allows for interface merging and accounts for the effect of possible pores on heat transfer. A complete description may be found in Delplanque et al. (1995) .

NUMERICAL ISSUES

The numerical approaches used for the fluid flow model and the solidification algorithm have been described elsewhere (Kothe and Mjolsness, 1992; Delplanque *et al.*, 1995) and will not be repeated here. However, the coupling of the solidification algorithm with the fluid flow solver raised some numerical issues which are discussed next.

The first issue is related to the local Stefan approximation. The amount of growth prescribed by the solidification model (Eq. 4) is a maximum value since the Stefan problem considers a semi-infinite domain (unlimited liquid). It must therefore be corrected to account for liquid availability. Hence, before moving a marker from its old location to the new one liquid availability is checked along the local solidification path ($\overline{n}$). If the path intersects a void, the marker position is set at the closest intersection to its old location.

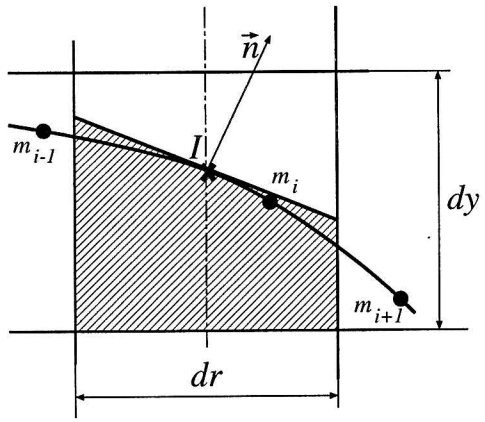

FIGURE 2: BUILDING INTERNAL OBSTACLES FROM LAGRANGIAN MARKER DATA.

Another important issue inherent to the present model is its hybrid Lagrangian/Eulerian nature. Since the solidifying solid is represented by internal obstacles to the fluid flow, it is necessary to translate the Lagrangian information provided by the markers into Eulerian data, the solid fraction distribution ($\gamma = 1 - \theta$). This transformation will result in volume conservation discrepancies which have to be minimized. The approach chosen is the following. First, the marker data is used to determine the logical coordinates of the interfacial cells. The value of γ in each of these cells is then obtained from the location of the intersection, I, of the interface with the vertical median of the cell and the normal, $\overline{n}$, to the interface at I. (cf. Fig. 2). $\overline{n}$ is obtained from the gradient of γ at the previous time-step, calculated using a 9-point interpolation formula. For added accuracy on the determination of the normal, two sweeps could be performed. Note also that the resulting new local solid fraction must always be less than one minus the old void fraction.

A major advantage of the Lagrangian/Eulerian approach, however, is its ability to simulate liquid-jet overflow, splashing, and the resulting non-connected solidified disk morphology. Solution techniques using deforming finite elements (Fukai *et al.*, 1993) are limited by their grid generation technique (Poulikakos and Waldvogel, 1995) which restrict their ability to simulate these phenomena, inherent to the high velocities encountered in spray atomization and deposition and plasma spraying.

All computations were performed on a DEC/Alpha 3000/500. Typically, the algorithm requires 3ms floating-point CPU per mesh point per time step. For the reference case defined below, this corresponds to 3.5 hours CPU for 422 cycles on a 132×72 mesh. The predominant time-step constraints are the Courant conditions.

RESULTS AND DISCUSSION

The parameters characterizing droplet spreading and solidification are (Delplanque and Rangel, 1995) the Reynolds number ($Re = \mathcal{V}D/\nu$), the Weber number ($We = \rho_\ell D\mathcal{V}^2/\sigma$), and the solidification constant (λ). The liquid/solid contact definitely plays an important role too (Bennett and Poulikakos, 1993). However, the motion of the contact line and the associated non-slip condition paradox are still unresolved problems (de Gennes *et al.*, 1990; Popov, 1992; Hocking, 1992; Anderson and Davis, 1994). Furthermore, the paucity of contact angle data and the many factors which affect them, such as solid surface roughness (Drelich and Miller, 1994) and mass transfer (Bourges and Shanahan, 1993), make it difficult to evaluate them properly at present.

A base case representative of practical spray deposition processes is defined: Re=25,000, We=1744, and λ=2. This case corresponds, for instance, to a 100μm tantalum droplet at 3250K (the melting point for tantalum) impinging on a 300K substrate at 50m/s. Without much reliable data available, the liquid/solid contact angle is taken to be 135^o and will be varied to investigate its influence.

The predicted behavior is shown in Figure 3. In this figure, the light shaded area represents the substrate while the dark shaded region represents the growing solid. The solid line is a VOF isopleth (0.75) and, although it gives a good indication of its location, it does not constitute a reconstruction of the free surface. Therefore, the small irregularities visible on the isopleth are only

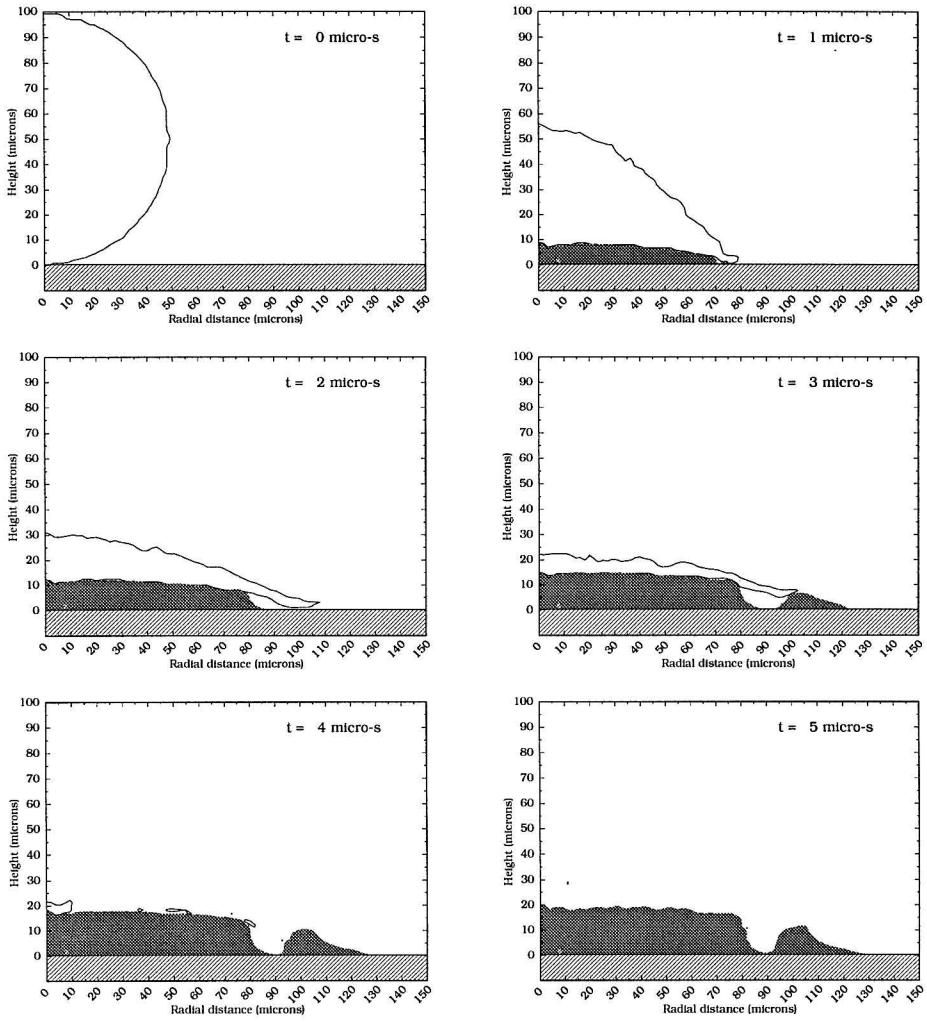

FIGURE 3: PREDICTED BEHAVIOR OF THE SPREADING AND SOLIDIFYING DROPLET AFTER IMPACT. REFERENCE CASE.

indicative of the small amount of smearing that the VOF field undergoes despite the second-order accurate advection scheme. It is believed that the perturbations introduced in the flow field by the growing solid are the source of this smearing since it is not observed in the absence of solidification. Similarly, the small floatsams and jetsams present towards the end of the solidification process are most likely caused by these perturbations.

The droplet initially spreads by a succession of small overflows, too small in fact to be well resolved. At 1.25μs, liquid-jet overflow is initiated. At 2.4μs, the liquid layer re-attaches on the substrate 13μm from the edge of the primary solidification disk where solidification starts. The growth of the secondary solidification ring narrows the trough initially created but at the end of solidification it is still 10μm wide and 11μm deep. In this case, the volume conservation discrepancy due to the above-mentioned Lagrangian/Eulerian transformation is about 7%. This is a typical value. Most of the error is produced after re-attachment and further successive mesh refinement in this region would reduce it. However, such a procedure would seriously affect the computational requirement of each case since several runs would be needed to refine the mesh.

The histories of the solid fraction (f_s) and the expansion coefficient ($\xi = 2R_s/D$, where R_s is the maximum radius of the solidified disk) are plotted in Figure 4. The plateau at 1.66 exhibited by ξ from 1.25μs to 2.4μs corresponds to the period of time during which the liquid jet overflows the solidified layer and extends radially outward without touching the substrate. During this time, solidification proceeds only vertically since there is no liquid/substrate contact that would result in radial growth of the solidified disk. This results in a somewhat lower total rate of solidification (df_s/dt).

Inada and Yang (1994) have recently observed this phenomenon experimentally. They used laser holographic interferometry to monitor the liquid/solid contact during the impact and

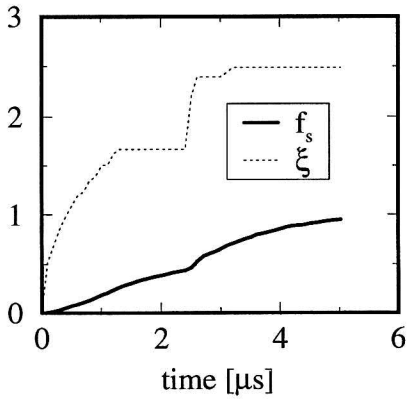

FIGURE 4: REFERENCE CASE. SOLID FRACTION AND SOLID RADIUS HISTORIES.

solidification of a lead droplet on a quartz substrate (Re=10,000; We=50; λ=1.27). The photographs that they obtained using a

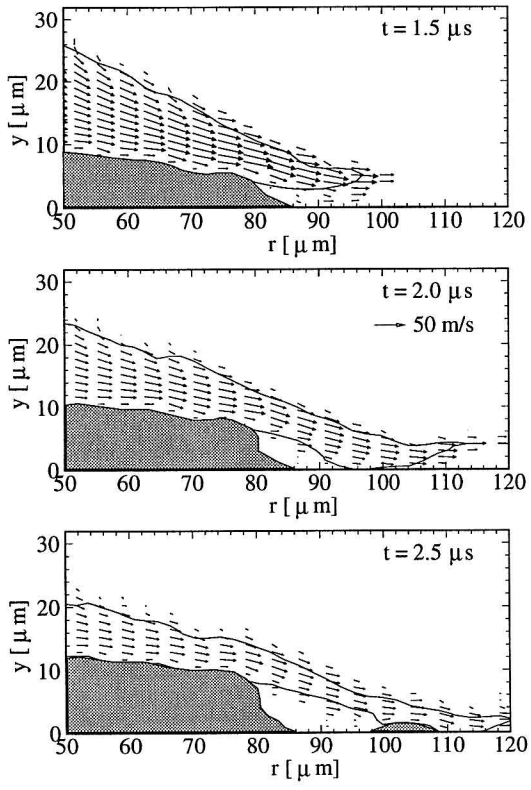

FIGURE 5: REFERENCE CASE. DETAIL OF THE LIQUID-JET OVERFLOW REGION.

high-speed camera clearly show the formation of a primary solidification disk which stops growing radially at about one fifth of the total solidification time, followed by what they describe as the "slipping of the molten phase at the interface" and "radial solidification." This radial layer is separated from the substrate by a thin layer of air which is apparent on Inada and Yang's photographs because its interference with the laser creates a so-called "Newton ring." However, Inada and Yang did not detect the secondary solidification ring.

A closer look at the overflow region (Fig 5) indicates that solidification rate, and radial and axial velocities are important factors in this phenomenon. The axial solid growth rate must be larger than the downward velocity for overflow to occur, while the magnitudes of the radial and axial velocities control the reattachment length.

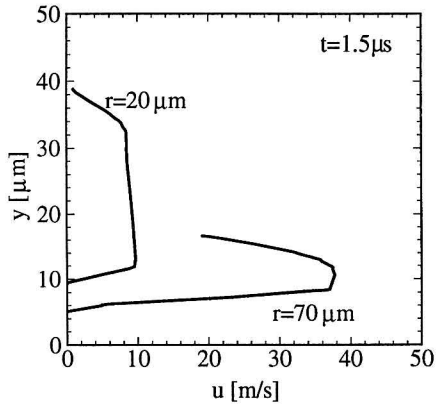

FIGURE 6: REFERENCE CASE. VELOCITY PROFILES AT TWO RADIAL LOCATIONS DURING LIQUID-JET OVERFLOW.

The axial profiles at $t = 1.5\mu$s of the radial velocity, u, at $r = 20\mu$m (droplet core) and $r = 70\mu$m (jet tip) show (Fig. 6) that u is about 4 times larger in the tip of the jet than in the core of the spreading droplet. However, liquid-jet overflow is not to be confused with the "sideway jetting" observed during high-velocity impact of non-solidifying droplets (Rein, 1993). Both phenomena are characterized by velocities high radial velocities in the region of the jet tip, but sideway jetting is the result of compressibility effects and impact shock wave propagation within the liquid, whereas liquid-jet overflow is essentially the result of the interactions of the fluid flow with the growing solid. Indeed, the numerical model used here neglects compressibility effects and yet liquid-jet overflow is predicted. In fact, liquid-jet overflow is a form of splashing which has been shown to be enhanced by surface roughness (Rein, 1993; Liu *et al.*, 1995). In this case, the growing solid introduces additional roughness thus promoting splashing.

Influence of Re, We, and λ

In order to determine how liquid-jet overflow is affected by each of the process parameters, the cases listed in Table 1 were considered. The corresponding predicted morphologies of the final solid disks are shown in Figure 7. The value of the contact

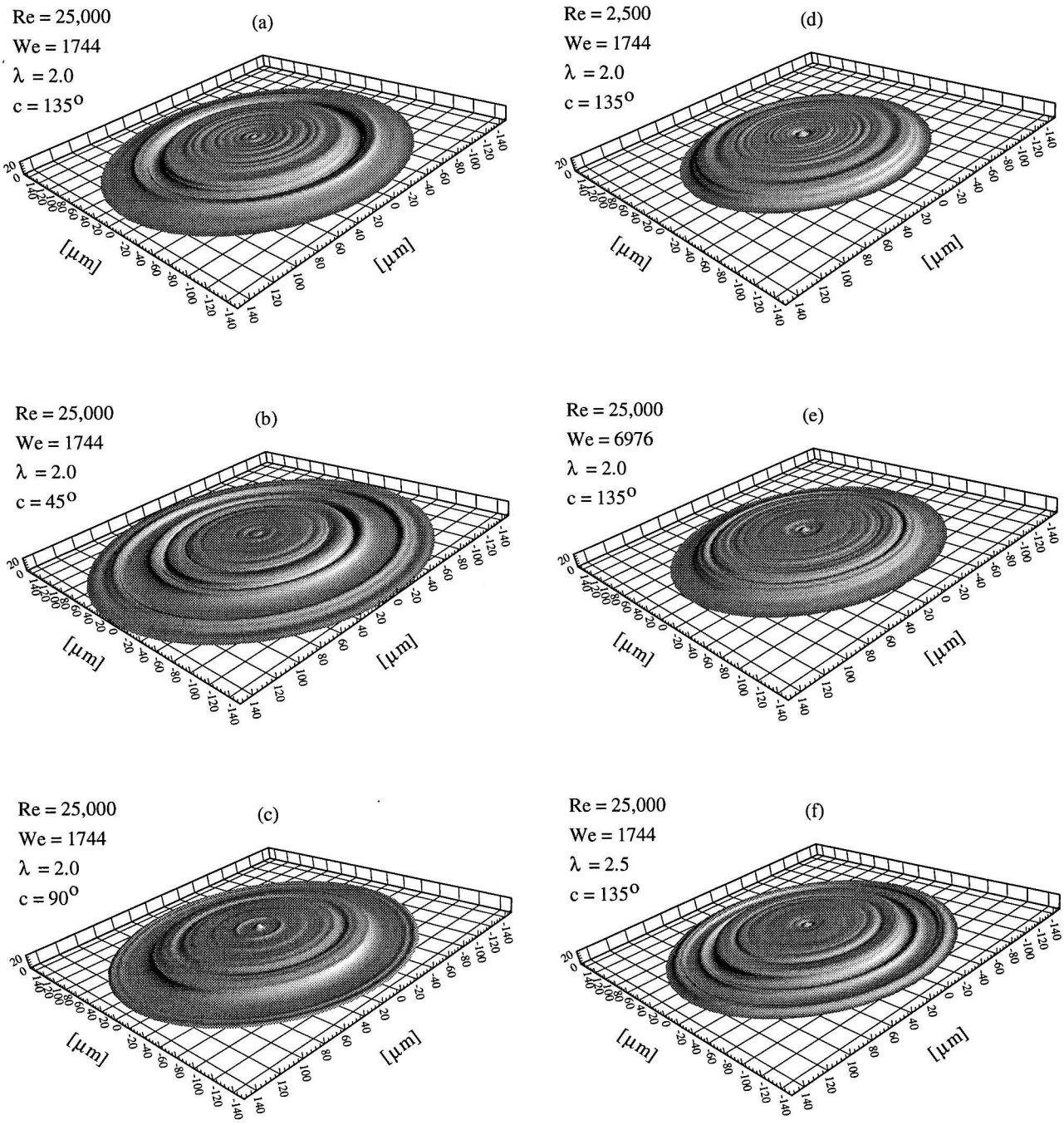

FIGURE 7: INFLUENCE OF Re, We, λ, and CONTACT ANGLE ON THE FINAL SOLID DISK MORPHOLOGY.

Case	Re	We	λ	c
a	25000	1744	2.0	135^o
b	25000	1744	2.0	45^o
c	25000	1744	2.0	90^o
d	2500	1744	2.0	135^o
e	25000	6976	2.0	135^o
f	25000	1744	2.5	135^o

Table 1: CASES CONSIDERED

angle is found to have a significant effect on both the solidification history and the final solid disk morphology. This is unfortunate since, as mentioned above, this property is extremely difficult to determine. Smaller contact angle yield a shorter re-attachment length but promote splashing, thus resulting in a rougher final morphology. This feature would promote the creation of pores as subsequent droplets impinge on this rough surface. Lower Reynolds number (case d) tend to reduce the occurrence of liquid-jet overflow because of the reduced liquid momentum, therefore resulting in a smoother solid disk. Note, however, that this disk also has a smaller radius (a lower Re reduces spreading) hence, it is thicker and it could enhance the formation of interstitial porosity. The effect of the Weber number is more complicated. One would expect higher Weber numbers, smaller surface tension coefficients, to promote liquid-jet overflow since less energy is required to increase the liquid surface area. In fact, the simulation (case e) show that because of the reduced surface tension, the liquid layer collapses early, therefore re-attaching much closer to the primary solidification disk than in the Reference Case (a). The resulting final disk is smaller and smoother than in the reference case. This demonstrates the important role of surface tension in the liquid-jet overflow phenomenon. Expectedly, higher solidification constants (case f) result in a more rapid growth of the disk thickness, thus enhancing liquid-jet overflow.

CONCLUSIONS

The impact, spreading, and solidification of a liquid-metal droplet on a flat substrate was investigated numerically. The solution procedure combined a multi-directional solidification algorithm with a Navier-Stokes solver for flows with free surfaces. The results show that, in the cases considered, which correspond to practical spray deposition processes, droplet spreading and solidification proceeds by a succession of fluid overflows: the liquid metal spreading on the solidifying disk flows over the edge of this disk and lands on the neighboring substrate where solidification is initiated. For high values of the solidification rate or the Reynolds number, the liquid-jet may land far enough (13μm for the 100μm diameter droplet considered in the base case) from the primary solid disk edge to result in the generation of a secondary solidification ring and, eventually, a trough in the final solid disk. However, larger Weber numbers could hinder the overflow mechanism by causing the liquid layer to collapse prematurely. The simulations also show that these behaviors are noticeably sensitive to the value of the liquid/solid contact angle used, therefore stressing the necessity of obtaining more accurate angle of contact data, and defining more accurate and workable contact line motion models.

ACKNOWLEDGMENT

This work was sponsored in part by by NSF (CTS 92-24850 and DMI 95-28684). This research was also supported in part by the University of California, Irvine through an allocation of computer resources.

REFERENCES

Anderson, D. M., and Davis, S. H., 1994, "Local fluid and heat flow near contact lines," *Journal of Fluid Mechanics*, Vol. 268, pp. 231–265.

Bennett, T., and Poulikakos, D., 1993, "Splat-quench solidification: estimating the maximum spreading of a droplet impacting a solid surface," *Journal of Materials Science*, Vol. 28, pp. 963–970.

Benz, M., Sawyer, T., Carter, W., Zabala, R., and Dupree, P., 1994, "Nitrogen in spray formed superalloys," *Powder Metallurgy*, Vol. 37, pp. 213–218.

Bourges, C., and Shanahan, M., 1993, "L'influence de l'evaporation sur l'angle de contact des gouttes d'eau," *C.R. Acad. Sci. Paris*, Vol. 316, pp. 311–316, Serie II.

Cai, W., Sickinger, A., Muehlberger, E., Bailey, D., and Lavernia, E. J., 1994, 1994 Internationa Conference on Tungsten and Refractory Metals, Washington, DC.

de Gennes, P. G., Hua, X., and Levinson, P., 1990, "Dynamics of wetting: local contact angles," *Journal of Fluid Mechanics*, Vol. 212, pp. 55–63.

Delplanque, J.-P., Lavernia, E. J., and Rangel, R. H., 1995, "Multi-directional solidification model for the description of micro-pore formation in spray deposition processes," *Numerical Heat Transfer, Part A: Applications*, Accepted for publication. Also presented at the 1995 ASME Winter Annual Meeting, November 12-17, San Francisco, California.

Delplanque, J.-P., and Rangel, R., 1995, "An improved model for droplet solidification on a flat surface," *Journal of Materials Science*, Submitted.

Drelich, J., and Miller, J., 1994, "The effect of solid surface heterogeneity and roughness on the contact angle/drop (bubble) size relationship," *Journal of Colloid and Interface Science*, Vol. 164, pp. 252–259.

Fukai, J., Zhao, Z., Poulikakos, D., Megaridis, C. M., and Miyatake, O., 1993, "Modeling of the deformation of a liquid droplet impinging on a flat surface," *Physics of Fluids*, Vol. 5, No. 11, pp. 2588–2599.

Hocking, L., 1992, "Rival contact-angle models and the spreading of drops," *Journal of Fluid Mechanics*, Vol. 239, pp. 671–681.

Inada, S., and Yang, W.-J., 1994, "Solidification of molten metal droplets impinging on a cold surface," *Experimental Heat Transfer*, Vol. 7, pp. 93–100.

Kothe, D. B., and Mjolsness, R. C., 1992, "RIPPLE – a new model for incompressible flows with free surfaces.," *AIAA Journal*, Vol. 30, No. 11, pp. 2694–2700.

Lavernia, E., and Wu, Y., 1995, *Spray Atomization and Deposition*, John Wiley & Sons, In Press.

Lavernia, E. J., 1989, "The evolution of microstructure during spray atomization and deposition," *International Journal of Rapid Solidification*, Vol. 5, No. 1, pp. 47–85.

Liu, H., Lavernia, E. J., and Rangel, R. H., 1993, "Numerical simulation of substrate impact and freezing of droplets in plasma spray processes," *J. Phys. D: Appl. Phys.*, Vol. 26, pp. 1900–1908.

Liu, H., Lavernia, E. J., and Rangel, R. H., 1994, "Numerical investigation of micro-pore formation during substrate impact of molten droplets in plasma spray processes," *Atomization and Sprays*, Vol. 4, pp. 369–384.

Liu, H., Lavernia, E. J., and Rangel, R. H., 1995, "Modeling of molten droplet impingement on a non-flat surface," *Acta Metallurgica et Materialia*, Vol. 43, No. 5, pp. 2053–2072.

Orme, M., 1993, "A novel technique of rapid solidification net-form materials synthesis," *Journal of Materials Engineering and Performance*, Vol. 2, No. 3, pp. 399–405.

Passow, C, H., Chun, J.-H., and Ando, T., 1993, "Spray deposition of a Sn-40 wt. pct. Pb alloy with uniform droplets," *Metallurgical Transactions A-Physical Metallurgy and Materials Science*, Vol. 24A, pp. 1187–1193.

Popov, V., 1992, "Effect of real wetting conditions on the hysteresis of the contact angle of drops," *Teplofizika Vysokikh Temperatur*, Vol. 30, pp. 915–923.

Poulikakos, D., and Waldvogel, J., 1995, "Transport phenomena relevant to the impact regime of the process of spray deposition; a review,", presented at the 24th National Heat Transfer Conference, Heat Transfer division of the ASME Portland, Ore.

Rangel, R., and Bian, X., 1996, "A metal-droplet deformation and solidification model with substrate remelting,", Submitted for presentation at the 1996 ASME IMECE, Second International Symposium on Multiphase Flows and Heat Transfer in Materials Processing, Atlanta, Georgia.

Rein, M., 1993, "Phenomena of liquid drop impac on solid and liquid surface," *Fluid Dynamics Research*, Vol. 12, pp. 61–93.

Sampath, S., and Herman, H., 1993, "Plasma spray forming metals, intermetallics, and composites," *JOM: The Journal of the Minerals, Metals & Materials Society*, Vol. 45, No. 7, pp. 42–49.

Sobolev, V., and Guilemany, J., 1994, "Investigation of coating porosity formation during high-velocity oxy-fuel (HVOF) spraying," *Materials Letters*, Vol. 18, pp. 304–308.

Trapaga, G., Matthys, E. F., Valencia, J. J., and Szekely, J., 1992, "Fluid flow, heat transfer, and solidification of molten metal droplets impinging on substrates — comparison of numerical and experimental results," *Metallurgical Transactions B-Process Metallurgy*, Vol. 23B, pp. 701–718.

Zhang, J., Gungor, M. N., and Lavernia, E. J., 1993, "The effect of porosity on the microstructural damping response of 6061 aluminum alloy," *Journal of Materials Science*, Vol. 28, No. 6, pp. 1515–1524.